# 微細構造特性評価のための暗視野落射照明系搭載ミューラー行列撮像偏光計顕微鏡システム開発

齋藤直洋，佐藤憲司，藤井　透，Heather Lynn Durko，Goldie Lynne Goldstein，Alton Hugh Phillips，Photini Faith Rice，Joceline Dominguez-Cooks，Gabrielle Vanessa Hutchens，Harrison Taylor Thurgood，Jennifer Kehlet Barton

# Mueller matrix imaging polarimeter microscope system development incorporating dark-field episcopic illumination system for microstructure characterization

Naooki SAITO, Kenji SATO, Toru FUJII, Heather Lynn DURKO, Goldie Lynne GOLDSTEIN, Alton Hugh PHILLIPS, Photini Faith RICE, Joceline DOMINGUEZ-COOKS, Gabrielle Vanessa HUTCHENS, Harrison Taylor THURGOOD and Jennifer Kehlet BARTON

偏光は，光と物質の相互作用を表す特徴量の一つである．偏光状態は，光学系が解像できないような微細構造でも反応して変化する．偏光イメージングは，多様な分野で容易に見ることができない情報を可視化するツールとなりつつある．我々は，物質と光の相互作用を記述できる16次元の情報をもつミューラー行列を計測できる顕微鏡の試作機を開発した．生体組織からの散乱光の偏光計測を行うことで，見た目には分からない組織構造の違いを識別することが可能である．このシステムは，落射暗視野偏光照明系とフルストークス撮像偏光計の構成されており，組織表面付近の構造により変化した散乱光の偏光状態を効率的に計測することができる．アリゾナ大学での長期的な実験検証を通じて，我々のシステムは高い安定性と共に信頼性を実証し，組織計測の結果は先行研究例と一致した．

Polarized light is one of the characteristic quantities representing the interaction between light and matter. The state of polarization changes in response to fine structures that cannot be resolved by an optical imaging system. Polarimetric imaging is becoming a tool in a variety of fields to visualize information that cannot otherwise be easily seen. We have developed a prototype microscope that can measure the 4×4 Mueller matrix that describes the interaction between matter and light. By performing the polarimetric measurement of the scattered light from the biological tissue, it is possible to discriminate a difference in the tissue structure that cannot be detected visually. This system, which comprises an epi-illumination dark-field polarized illumination system and a full-Stokes imaging polarimeter, can efficiently measure the polarization state of light scattered by the structure near the tissue surface. Through long-term experimental validation at the University of Arizona, our system has demonstrated reliability with high stability, and tissue measurement results are consistent with those reported in the literature.

## *1* Introduction

Polarimetric imaging enables us to detect information that is not visually apparent. It is well known that the state of polarization (SOP) of light can change as it transmits through, reflects from, or scatters within an object due to the object's optical properties, surface features, and microscopic structures[1]. Therefore, techniques to visualize polarization information have been developed for many fields.

Combining microscopy and polarimetry can create a pow-erful tool for optical measurement. Microscopes are high-precision and highly reliable optical measurement devices having both an illumination system and an observation system[2], and can be employed for industrial as well as bio-medical applications.

Many attempts to utilize polarimetry in the medical field have been studied[1,3,4]. Most commonly, it is employed to detect cancerous tissues for early cancer diagnosis. With the resolution of standard cancer detection methods such as CT, MRI, and PET, it is not easy to visualize cancerous regions

smaller than 1 mm in size. Discriminating and detecting microscopic cancer tissue can lead to early cancer detection and contribute to improved five-year survival rate.

Nikon Corporation has developed a microscope system to identify differences in the microstructure of biological tissue using polarimetry to detect early cancer[5]. Proper control of the SOP of the illumination light on the sample makes it possible to measure a Mueller matrix that describes the complex interaction between the sample and polarized light. The realization of the Mueller matrix measurement in a microscope system can provide a quantitative polarization measurement environment that cannot be achieved with a conventional polarization microscope. The system performance was verified and a tissue study was performed in collaboration with the University of Arizona.

# 2 Principle and Methods

## (1) System concept

The configuration of the Mueller matrix polarimeter can be conceptualized as shown in Fig. 1[6]. For the Mueller matrix measurement, the optical system consists of two essential parts: a polarization state generator (PSG) that illuminates the sample on the sample stage with known polarization states, and a polarization state analyzer (PSA) that measures the SOP of the scattered light from the sample as Stokes parameters. The Mueller matrix of the sample can be estimated using the Stokes parameter information obtained under a plurality of polarized illuminations.



$$\mathbf{S}_{detector} = \mathbf{M}_{PSA}\mathbf{M}_{sample}\mathbf{M}_{PSG}\mathbf{S}_{source}$$

*1: Polarization state generator
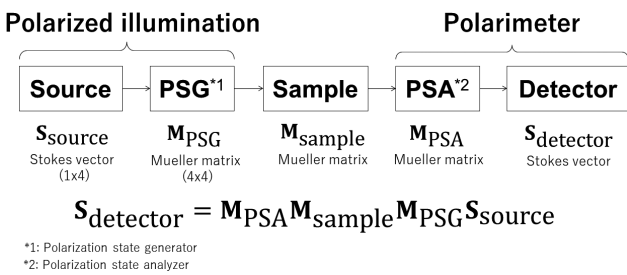*2: Polarization state analyzer

Fig. 1   The schematic of Mueller matrix polarimeter

Image contrast of the microstructure near the surface of the tissue sample can be enhanced by using dark-field epi-illumination, which prevents specular reflections from contributing to the polarimetric measurements. Epi-illumination can also be used to measure the surface of thick tissue samples, which accommodates a variety of sample forms without the need for sample slide preparation.

Multispectral measurements can take advantage of the difference in tissue light absorption. The light absorption coefficient of hemoglobin contained in biological tissue varies across the visible spectrum. At shorter wavelengths, the appearance of the tissue surface and the presence of blood can be revealed. At longer wavelengths, we can image deeper into the tissue. Spectral imaging can also provide information that is relevant to tissue identification tasks.

The imaging polarimeter incorporated in the observation path collects the full Stokes measurement in a single image. In the conventional method, the Stokes vector is measured by mechanically or electrically modulating the polarization of the measured light and acquiring a plurality of images. Fig. 2 shows the imaging polarimeter using the modified Savart plates (MSPs) in this optical system[7][8].
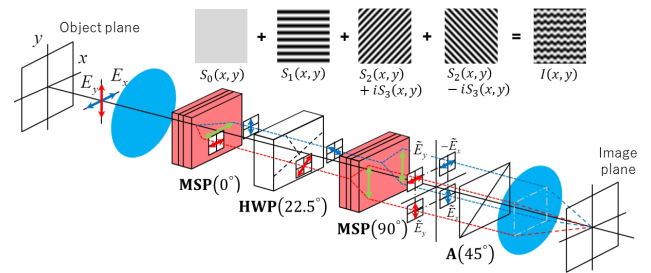


Fig. 2   Full-Stokes Imaging Polarimeter

The imaging polarimeter module generates polarization-dependent interference carrier fringes, so that all Stokes parameters can be encoded into one image. With this approach, since there are no mechanical moving parts or electrical modulation, stable and high-speed Stokes measurements are achieved.

## (2) Mueller matrix imaging polarimeter microscope

We prototyped an optical system that combines a dark-field epi-illumination polarization generator with a polarizing microscope and a full-Stokes polarimeter. The system was constructed using a modified Nikon ECLIPSE LV100N POL polarizing microscope.

The PSG is incorporated as part of an epi-illumination system in which the outer NA of the objective lens pupil are used to realize a dark-field epi-illumination system. An incoherent illumination light source (SPECTRA X Light Engine, Lumencor) connects to the epi-illumination path with an optical fiber. The light source has can select between five bands with center wavelengths at 405 nm, 442 nm, 473 nm, 543 nm, and 632 nm. Interference filters constrain each band to 3 nm widths.

In the epi-illumination system, an arbitrary polarization is controlled by a combination of one polarizer and one quarter-wave plate. Each polarizing element is mounted on a rotary stage (K10CR1A2/M, Thorlabs, Inc.) to set an arbi-

trary azimuthal angle. Achromatic quarter-wave plates (APSAW-5, Astropribor) are employed to provide stable performance within the operating wavelength range.

The position of the light source fiber corresponds to the illumination path position in the pupil of the objective lens. In practice, the position of the fiber end is optimized to couple into the outer NA of the objective lens while minimizing stray light in the PSG optics. Fig. 3 shows the microscope and a diagram of the optical path.
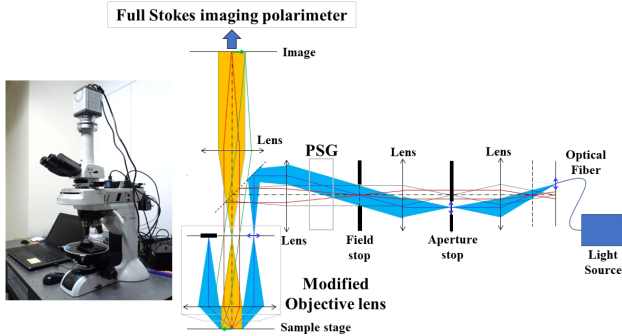


Fig. 3   Mueller matrix polarimeter microscope (left), and dark-field epi-illumination and observation optical paths (right)

Dark-field illumination is achieved by passing light from the illumination system through an aperture defined by a mask at the objective lens pupil. The specular reflected light on the sample surface is blocked by the pupil mask. Only polarized light scattered by the fine structure on the sample surface can enter the observation optical path through the central NA of the objective pupil.

The modified objective lens enables both dark-field epi-illumination and polarimetry of scattered light from the sample. The center NA of the pupil of the objective lens and the polarimeter installed on the camera adapter play the role of PSA. We modified a Nikon brightfield objective lens (Nikon CFI TU Plan Fluor EPI 5×, 10×) with minimal polarization distortion. The performance parameters after modification are as shown in Table 1.

The imaging polarimeter module uses modified Savart plates to enable snapshot measurements of Stokes parameters from polarized light that scatters from the sample. Two MSPs (Kogakugiken Corp.) installed in the camera adapter realize the separation of polarization components and the spatial shear with minimal crosstalk. A scientific CMOS camera (2048×2048-pixel, ORCA Flash 4.0, Hamamatsu Photonics K. K.) is positioned at the image plane to detect polarization-dependent interference fringes with high sensitivity and low noise. The spatial frequency of the interference fringes is set by the wavelength-dependent shear in the Savart plates, which determines the spatial resolution of the polar-

Table 1   System specifications

| Parameter | Specification | |
|---|---|---|
| Illumination | | |
| Wavelength | 405, 442, 473, 543, 633 nm (limited by interference filter; FWHM < 3 nm) | |
| State of polarization | Automatically switched by software | |
| | | |
| Imaging | 5 × objective | 10 × objective |
| Effective magnification | 3 × | 6 × |
| Field of view (mm) | 3.67 | 1.83 |
| Working distance (mm) | 23.5 | 17.5 |
| Imaging NA (Max.) | 0.075 | 0.150 |
| Illumination NA (Max.) | 0.150 | 0.300 |
| | | |
| Polarimeter | 5× objective | 10× objective |
| Spatial resolution | 9.8 μm (at 442 nm) 10.6 μm (at 543 nm) 14.5 μm (at 632 nm) | 4.9 μm (at 442 nm) 5.3 μm (at 543 nm) 7.3 μm (at 632 nm) |
| Sensor | 2048 × 2048 pixels, 13.312 × 13.312 mm | |

ization measurement. The spatial resolutions are provided in Table 1.

Full Mueller matrix measurements can be automatically obtained by this system. The custom software and external PC control the wavelength and SOP of the illumination light and automatically perform a series of Stokes parameter measurements required for Mueller matrix calculations. A similarly automated post-imaging process computes Mueller matrix maps of the imaged sample from the measured images at each measured wavelength.

Polarization errors caused by the optical system have been characterized through calibration and are removed from the sample measurements.

# *3* Stability enhancement

Because the MSP-based polarimeter used in this system encodes the Stokes parameters into the polarization-dependent carrier fringes, to determine the Stokes parameters from each measured image, the phase components of the carrier fringes are extracted relative to a reference measurement of a known SOP that is performed in advance of the sample measurement. If the polarimeter imaging environment does not change, the carrier phase components of the spatial carrier fringes remain constant. However, thermal variations in the imaging environment can change the carrier phase components between the reference measurement and the sample measurement, the demodulated information includes an error component corresponding to the mismatch in carrier phases.

We developed a model for the variation of spatial carrier fringes caused by temperature disturbances and developed a method to reduce the errors. The amount of shear generated in the birefringent crystal plates in the MSP is temperature-dependent. When the temperature changes, so does the carrier phase determined by the shear amount of the MSP. If a temperature disturbance occurs between the reference measurement and the sample measurement, the carrier phase component cannot be properly removed. Factors that cause a temperature disturbance include temperature changes in the room where the microscope is installed, and exhaust heat from the scientific CMOS camera. We identified the fringe fluctuation caused by the camera exhaust and removed the effect with post-processing compensation.

Through experiments and data analysis, we analyzed influence of each potential source or error by extracting the fringe variation error measured by the microscope system and performing quantitative analysis. From the analysis results, it was found that the errors caused by the vibrations caused by the operation and refocusing of the stage and the errors caused by the exhaust heat of the cooling camera were the dominant factors. We reduced the Mueller matrix element error caused by the temperature-dependent phase shift of the carrier fringes, improving the measurement stability. Table 2 compares the variation ($3\sigma$) of the average value across the field of view of the Mueller matrix error before and after the fluctuation compensation for each error factor. Regarding the error due to thermal fluctuation, the post-processing reduced the Mueller matrix element $3\sigma$ error from $0.046$ to $0.021$. Furthermore, by incorporating a function to monitor the fringe position, the error is expected to be suppressed to $0.010$ or less.

Table 2 Comparison of Mueller matrix error of the system between before and after stability compensation

| Error factors | Mueller matrix error ($3\sigma$) | |
| --- | --- | --- |
| | Before compensation | After compensation |
| Repeatability + Resetability of automated contol | 0.002 | 0.002 |
| Temperature fluctuation | 0.042 | 0.007 |
| Resetability of objective revolver | < 0.001 | < 0.001 |
| Resetability of rotational stage | 0.018 | 0.019 |
| Resetability of standard element | 0.004 | 0.004 |
| Mueller matrix error of whole system | 0.046 | 0.021 |

# *4* Results

We measured Mueller matrices of some biological samples using the prototype system.

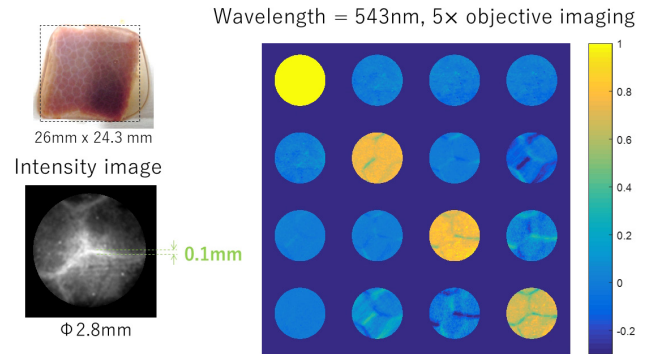Fig. 4 shows an example of measurement of porcine liver as a biological tissue sample.



Fig. 4 The photo of porcine liver (upper left), the $m_{00}$ microscope image at 543 nm (lower left), and the $m_{00}$-normalized measured Mueller matrix map

A color map of the Mueller matrix elements is shown. The Mueller matrix is normalized by the $m_{00}$ intensity so that the polarization characteristics are displayed in an easy-to-understand manner. Porcine liver comprises many hepatic lobules surrounded by connective tissue. The connective tissue is known to have birefringent properties. In the $m_{00}$ image, the connective tissue appears white, but in the Mueller matrix visualization, the same regions are represented in various colors that relate to the microscopic orientation of the birefringent tissue.

The polarization characteristics differ depending on the alignment direction of the connecting tissue, and the values of the Mueller matrix differ accordingly. This result indicates that the measurement and discrimination of the polarization characteristics of the submicron-sized tissue structure can be acquired with a Mueller matrix measurement.

We investigated the performance of this polarimeter microscope system by using it for cancer tissue imaging studies in collaboration with the research group led by Professor Jennifer Barton at the University of Arizona (Tucson, AZ USA).

Samples were obtained from discarded surgical resections of human colon tissue. The samples are cut from the discarded tissue immediately after the operation. Sample sections were obtained from visibly diseased and healthy tissue regions. Each sample is examined for the condition of the cancer tissue in pathological diagnosis after microscopic observation.

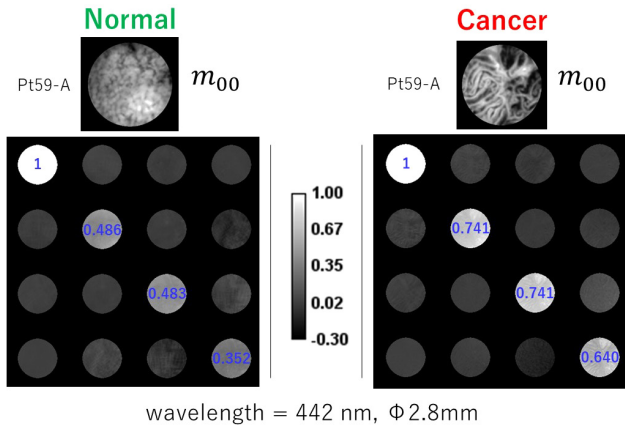Fig. 5 shows an example of Mueller matrix measurements

**Fig. 5** $m_{00}$-normalized Mueller matrix maps of normal (left) and cancerous (right) human colon tissue

of normal and cancerous human colon tissue obtained from one patient and illuminated with 442 nm light. The average value across the field of view of the diagonal elements of the Mueller matrix is shown in blue. The intensity image shows the morphology of the samples, which are characteristic of each type of tissue. For both types of tissue, the diagonal components are dominant. However, cancerous tissue tends to have larger diagonal element values.

We compared the diagonal values using data from multiple patients. Fig. 6 shows the distribution of the Mueller matrix measurement results for multiple human colon tissues.
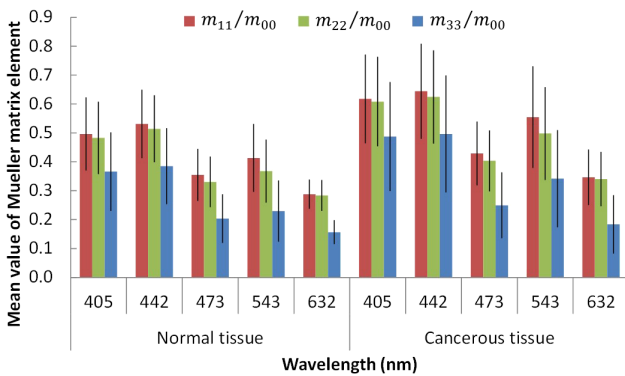


**Fig. 6** The statistics of the diagonal element values across the field of view of the Mueller matrix for 18 patients, mean value and standard deviation

We calculated the statistics of the mean value across the field of view of the Mueller matrix element values of multiple patients. In Fig. 6, each color is the average of each diagonal element value at the five wavelengths. Black bars indicate the standard deviation among 18 patients.

From these results, although the variation between patients is large, the diagonal element values of the Mueller matrix tend to be larger in cancer tissues than in normal tis-

sues. This result is consistent with previous studies reported by Novikova[9]. The colon-tissue Mueller matrices obtained with this microscope have also been utilized for additional related studies[10].

# 5 Conclusion

We developed a novel Mueller matrix polarimeter microscope system that consists of a dark field epi-illumination system and a full-Stokes imaging polarimeter. The dark-field observation provided by the combination of the epi-illumination system and the modified objective lens performs polarization measurements of the light scattered from thick biological samples. The software automatically controls the illumination wavelength and SOP, and measurements acquired from a set of incident SOPs provide sufficient information to calculate the Mueller matrix of a sample at several wavelengths. The polarization error of the optical system in the system is minimized with calibration, and errors from thermal fluctuations can be stably reduced.

We have shown the effectiveness of the microscope system in biological tissue experiments. The Mueller matrix measurements of porcine liver tissue indicate an increased contrast between microscopic tissue structures when measured by the difference in polarization state. The statistical difference between the Mueller matrices of cancer and normal tissues in human colon replicated the results of previous studies and proved the validity of the system. Through this research, we showed the possibility of a new medical imaging technology using polarized light.

## References

1) V. V. Tuchin, L. Wang and D. A. Zimnyakov: *Optical Polarization in Biomedical Applications* (Springer Science & Business Media, 2006).

2) S. Schwartz, S. Ross, K. Spring, T. Fellers, M. Parry-Hill, D. Murphy, J. Lippincott-Schwartz, G. Patterson, D. Piston and M. Davidson: *Nikon MicroscopyU*, https://microscopyu.com/ (2005).

3) Z. Chen, Y. Yao, Y. Zhu and H. Ma: "A colinear backscattering Mueller matrix microscope for reflection Muller matrix imaging", *SPIE Proceedings*, 104890M (2018).

4) T. Novikova, J. Rehbinder, S. Deby, H. Haddad, J. Vizet, A. Pierangelo, P. Validire, A. Benali, B. Gayet, B. Teig, A. Nazac, B. Drévillon, F. Moreau and A. De Martino: "Multispectral Mueller Matrix Imaging Polarimetry for Studies of Human Tissues", *OSA Technical Digest* (online) (Optical Society of America, 2016), paper TTh3B.2. (doi: 10.1364/

TRANSLATIONAL.2016.TTh3B.2)

5) N. Saito, K. Sato, T. Fujii, H. L. Durko, G. L. Goldstein, A. H. Phillips, J. Dominguez-Cooks, G. V. Hutchens, H. T. Thurgood, P. F. Rice and J. K. Barton: "Multispectral Mueller matrix imaging dark-field microscope for biological sample observation", *SPIE Proceedings*, 108901A (2019).

6) D. H. Goldstein: *Polarized Light*, 3rd ed. (CRC press, 2010).

7) K. Oka and N. Saito: "Snapshot complete imaging polarimeter using Savart plates", *SPIE Proceedings*, 629508 (2006).

8) N. Saito, S. Odate, K. Otaki, M. Kubota, R. Kitahara and K. Oka: "Wide field snapshot imaging polarimeter using

modified Savart plates", *SPIE Proceedings*, 88730M (2013).

9) T. Novikova, A. Pierangelo, S. Manhas, A. Benali, P. Validire, B. Gayet and A. De Martino: "The origins of polarimetric image contrast between healthy and cancerous human colon tissue", *Applied Physics Letters*, 102 (2013) 241103.

10) T. Fujii, Y. Yamasaki, N. Saito, M. Sawada, R. Narita, T. Saito, D. L. Heather, P. F. Rice, G. V. Hutchens, J. Dominguez-Cooks, H. T. Thurgood, S. Chandrae, V. Nfonsam and J. K. Barton: "Polarization characteristics of dark-field microscopic polarimetric images of human colon tissue", *SPIE Proceedings*, 108902J (2019).

齋藤直洋
Naooki SAITO
研究開発本部
光技術研究所
Optical Research Laboratory
Research and Development Division

佐藤憲司
Kenji SATO
FPD 装置事業部 開発統括部
第二開発部
2nd Development Department
Development Sector
FPD Lithography Business Unit

藤井　透
Toru FUJII
研究開発本部
光技術研究所
Optical Research Laboratory
Research and Development Division

Heather Lynn DURKO
Nikon Research Corporation of America

Goldie Lynne GOLDSTEIN
Nikon Research Corporation of America

Alton Hugh PHILLIPS
Nikon Research Corporation of America

Photini Faith RICE
The University of Arizona

Joceline DOMINGUEZ-COOKS
The University of Arizona

Gabrielle Vanessa HUTCHENS
The University of Arizona

Harrison Taylor THURGOOD
The University of Arizona

Jennifer Kehlet BARTON
The University of Arizona